ADVANCED FUNCTIONAL MATERIALS
www.afm-journal.de

Palladium-Based Metallic Glass with High Thrombogenic Resistance for Blood-Contacting Medical Devices

Martina Cihova, Eike Müller, Yashoda Chandorkar, Kerstin Thorwarth, Giuseppino Fortunato,† Katharina Maniura-Weber, Jörg F. Löffler, and Markus Rottmar**

Advancements in the design of mechanical blood circulatory devices have greatly improved patient survival rates, but currently employed metals still provoke a thrombosis response upon contact with blood, with potential life-threatening consequences. While coating strategies have been developed to address this limitation, they possess inherent drawbacks such as susceptibility to crack formation and delamination. Herein, an amorphous metal based on palladium (Pd) is scrutinized and reveals substantial thrombogenic resistance compared to a state-of-the-art titanium alloy. In vitro assessment with human whole blood shows that the Pd glass provokes reduced platelet activation (lower expression of CD62P, CD41/CD61) and greatly retarded fibrin formation, but pronounced platelet spreading therewith challenging the dogma that platelet spreading equals activation. Mechanistic analysis of the early biomaterial–blood interactions reveals that conformational changes of adhered fibrinogen, and modified $\alpha_{IIb}\beta_3$ integrin expression and distribution across adhered platelets, underlay the superior performance of Pd glass. The study is accompanied by structural and thermophysical bulk investigations and physicochemical surface characterization to link the materials properties with the observed blood response. The results reveal a remarkable potential of Pd-based glass as direct blood-contacting bulk material without the need for coating.

1. Introduction

The material of choice for blood-contacting medical devices is typically of polymeric, low-surface energy and hydrophobic nature, such as provided by silicones, polyurethanes, or fluoropolymers.[1] However, metallic materials are required when the devices or parts require high strength, stiffness or cyclic-loading fatigue resistance, such as in ventricular assist devices (VADs) or total artificial hearts (TAHs). In these mechanical circulatory support systems, crystalline Ti–Al6–V4 (in wt%, Ti64) is still the first material of choice.[2] Even though Ti64 has demonstrated excellent biocompatibility, it exhibits a high level of thrombogenicity[3] that challenges its application in blood-contacting devices. Thrombosis and thromboembolism, as well as bleeding complications arising from the need of anticoagulation and antiplatelet medication, are thus major constraints in mechanical circulatory support therapy. The lack of suitable metallic bulk-material alternatives has navigated the focus toward strategies of surface engineering, mainly on topographical cues, and coatings to achieve improved hemocompatibility.[4–7] Among the antithrombogenic coatings, bioactive heparin[6] and inorganic diamond-like carbon (DLC)[7] are the largely prevailing gold standards of blood-contacting surfaces.

While the various coating strategies immensely improved surface hemocompatibility, their use is not unreservedly

M. Cihova,[+] J. F. Löffler
Laboratory of Metal Physics and Technology
Department of Materials
ETH Zurich
8093 Zurich, Switzerland
E-mail: m.cihova@imperial.ac.uk

The ORCID identification number(s) for the author(s) of this article can be found under https://doi.org/10.1002/adfm.202108256.

[+]Present address: Department of Materials, Imperial College London, London SW7 2AZ, UK

†Deceased

E. Müller, Y. Chandorkar, K. Maniura-Weber, M. Rottmar
Laboratory for Biointerfaces
Empa
Swiss Federal Laboratories for Materials Science and Technology
9014 St. Gallen, Switzerland
E-mail: markus.rottmar@empa.ch

K. Thorwarth
Surface Science & Coating Technologies
Empa
Swiss Federal Laboratories for Materials Science and Technology
8600 Dübendorf, Switzerland

G. Fortunato†
Laboratory for Biomimetic Membranes and Textiles
Empa
Swiss Federal Laboratories for Materials Science and Technology
9014 St. Gallen, Switzerland

DOI: 10.1002/adfm.202108256

positive. Mechanical mismatch between the coating and bulk material may result in crack formation, and the cracks or imperfections may cause coating breakdown or delamination.[8] Surface imperfections, such as roughness, kinks, or crevices, may also give rise to disturbed blood flow or stasis, inducing blood cell activation.[9] Bioactive coatings, for example, heparin, are additionally limited in their lifetime owing to natural degradation of the bioactive compound[4] or depletion of noncovalently bound substances. With limited coating durability being detrimental for the long-term success of the device, there is an urgent demand for new hemocompatible bulk metals.

In this study, we propose a bulk metallic glass (BMG) as biometal for blood-contacting devices. Metallic glasses reveal an amorphous, i.e. disordered, atomic arrangement, resulting from rapid cooling of the melt as to suppress the formation of crystalline phases.[10] The absence of structural heterogeneities such as grain boundaries and crystal defects, which may both be considered structural weak points in crystalline alloys, results in mechanical properties and corrosion resistance of BMGs superior to their crystalline counterparts. In fact, BMGs display high strength (yield strengths two to three times higher compared to their crystalline counterparts)[11] and elasticity (elastic strain limit at about 2% compared to <<1% for their crystalline counterparts),[12] enhanced resistance to heterogeneous microgalvanic corrosion,[13,14] and improved wear resistance.[15] It is thus not surprising that the unique combination of properties known for BMGs motivates research on their potential for biomedical applications.[16–18] In the context of blood-contacting devices, BMGs have mostly been investigated for their application as cardiovascular stents,[19–21] with an emphasis on the material's fatigue resistance under cyclic load[21] and the ability for self-expansion.[19] Biological compatibility testing typically concerned cytocompatibility or toxicity, while BMGs' potential as blood-contacting materials was evaluated in light of hemolysis[22] rather than thrombogenicity and has so far been limited to studies of isolated material–protein[23,24] or material–platelet interactions.[25] To our knowledge, no BMG has so far been investigated for the complex and multiparameter requirements that a hemocompatible material must fulfill.

Here, we scrutinize a palladium (Pd)-based BMG for its suitability to be used in blood-contacting devices. We chose Pd as the base material because of its wide use as a biometal. For instance, Pd is used in dentistry as dental prostheses, typically alloyed with copper (Cu, typically 5–10 wt%), gallium or tin.[26] As such, it convinces with good biocompatibility, high strength, high corrosion resistance, radiopacity,[27] and MRI compatibility owing to its low magnetic susceptibility.[26] As for its hemocompatibility, pure crystalline Pd was shown to stimulate significantly lower levels of thrombin–antithrombin (TAT)-complex generation and lower platelet depletion from whole blood compared to Ti.[28]

Following the established use of crystalline Pd-based alloys, we chose the metallic glass $Pd_{77.5}Si_{16.5}Cu_6$ (in at%), corresponding to Pd90.7–Si5.1–Cu4.2 (in wt%). Discovered in 1969[29] and optimized toward bulk thickness in the 1970s,[30] this BMG combines a large compressive plastic strain of 11%,[31] high thermal stability,[32] and a critical casting thickness of 15 mm.[32] Despite this alloy being one of the oldest BMGs, its potential as a biomaterial per se and as a biomaterial for blood-contacting devices in particular has thus far not been investigated.

In this study, we comprehensively investigated the Pd-based BMG for its hemocompatibility. Following thorough characterization of the material's bulk and surface properties, we explored the thrombogenic potential of Pd-based glass in contact with partially heparinized human whole blood, using the state-of-the-art crystalline Ti64 bulk metal as reference material, according to the ISO 10993-4 guidance on the choice of controls.[33] Pd-based glass was further compared with other BMGs of varying chemical compositions based on Ti or Zr, and benchmarked against an amorphous DLC coating, presenting today's gold standard in mechanical circulatory support systems.

In a rationally designed approach, we systematically demonstrate how the materials' physico-chemical properties balance blood coagulation on the different surfaces and reveal potential biological mechanisms. We relate the material-surface properties to the amount and conformation of the plasma protein fibrinogen, morphology of adhered platelets as well as their activation status, fibrin formation, and molecular markers of blood coagulation.

2. Results and Discussion

2.1. Whole Human Blood Response to Amorphous Pd in Comparison to Crystalline Ti64

As a first step, we aimed at benchmarking the blood response to Pd-based glass against state-of-the-art crystalline bulk metal Ti64. Prior to this, the materials' microstructure was analyzed using scanning electron microscopy (SEM) and X-ray diffraction (XRD) (**Figure 1**B,C), carefully examining the as-cast Pd glass for inhomogeneities. Backscattered-electron (BSE) contrast, which is sensitive for atomic number (*Z*), reveals microstructural uniformity without any resolvable phases (Figure 1B, left). Sporadically, small pores were observed, which may result from the casting in boron oxide (dark spot on the SEM image in Figure 1B, left). Because the pore density was very low, with only few pores per sample surface, they were not further considered. The samples' amorphous structure was verified by XRD (Figure 1C, top). In fact, the obtained XRD pattern shows only two diffuse halos, resulting from the short-range order of the alloy, with no trace of crystalline peaks. The microstructure of the Ti64 alloy is characterized by the presence of various phases, evident from different grey tones in the BSE contrast (Figure 1B, right). The corresponding XRD pattern (Figure 1C, bottom) shows well-defined Bragg peaks as expected for crystalline materials.

To investigate the materials' thrombogenic potential, the Pd-glass and Ti64 substrates were incubated up to 48 min in partially heparinized human whole blood and evaluated for platelet adhesion and thrombus formation (Figure 1D–F).

The incubation was performed in vitro in polytetrafluoroethylene (PTFE) devices under exclusion of air contact and under dynamic conditions (orbital shaker). Materials were brought in contact with freshly withdrawn, partially heparinized human whole blood, and the blood responses evaluated

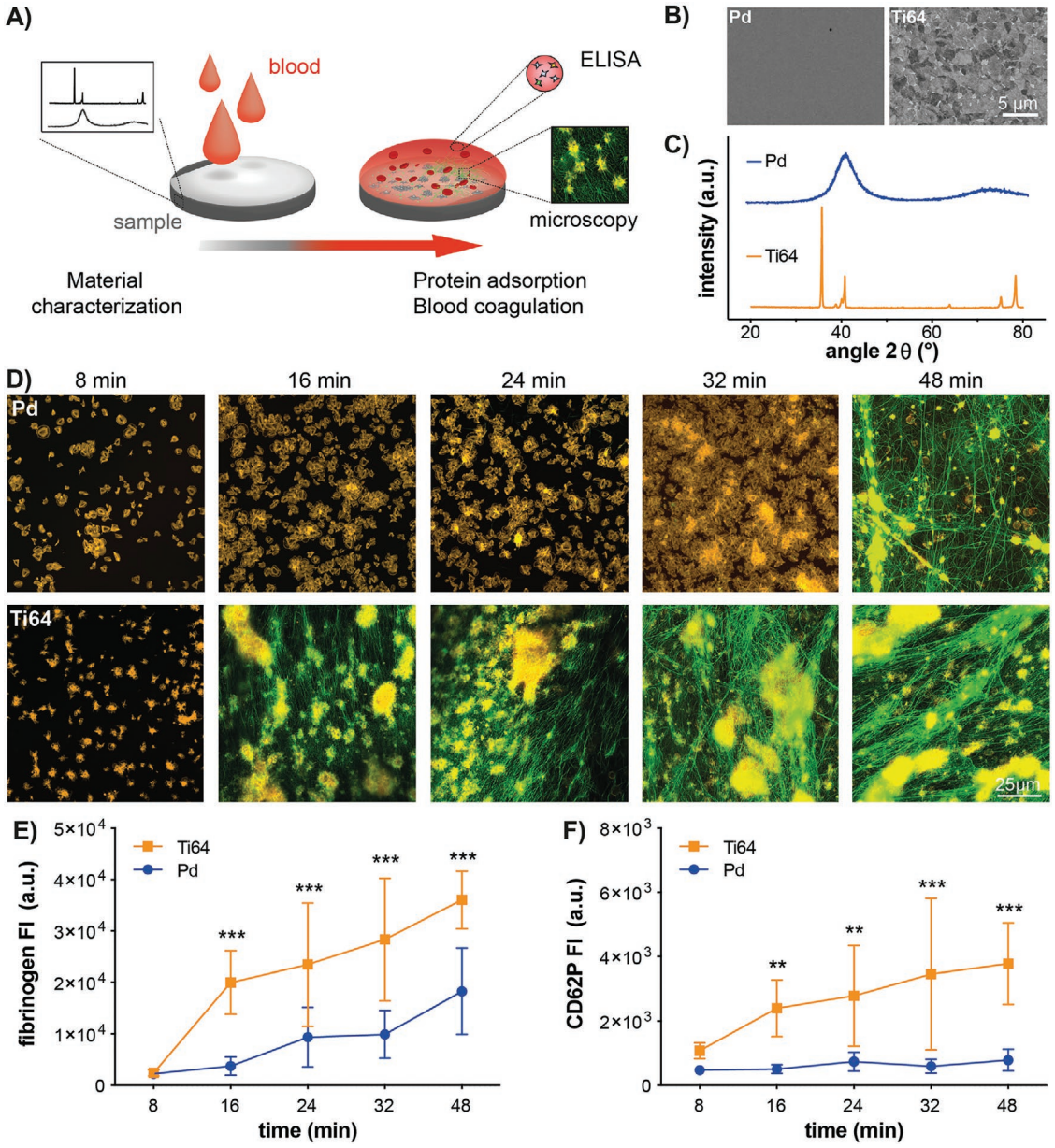

Figure 1. Blood coagulation on the surfaces of Pd glass and crystalline Ti64 after incubation in partially heparinized whole blood. A) Schematic illustration of the experimental protocol. B,C) Material structure characterized by B) SEM-BSE imaging and C) XRD. D) Representative CLSM images of blood coagulation as a function of surface and incubation time. Samples were stained for platelet cytoskeletal actin (orange) and fibrin (green); the yellow color results from an overlaid signal of orange and green. E) Amount of fibrinogen, FG, and F) amount of CD62P (platelet activation marker) expressed on the different surfaces after incubation in whole blood. Note that FG marks both, the FG adhered to the biomaterial surfaces and the formed fibrin fibers that result from enzymatic conversation of the fluorescently labeled FG. Fluorescence intensities, FI, were quantified using a microarray scanner. Data are presented as mean ± SD for $n = 4$. Asterisks denote statistical significances as follows: $^{**}p < 0.01$ and $^{***}p < 0.001$.

via enzyme-linked immunosorbent assays (ELISA) (supernatant analysis) and immunohistochemical staining and confocal laser scanning microscopy (CLSM) (analysis of surface-adhered compounds) (Figure 1A). The CLSM images in Figure 1D show the evolution of adhered platelets (actin in orange) and fibrinogen (FG) (in green) on top of the surfaces for increasing incubation times (see Figure S1, Supporting Information, for split channels of actin and FG). For both materials, platelet adhesion to the respective surface was observed after 8 min of incubation. While the CLSM images indicate a similar number of adherent platelets on both materials, their morphology appeared distinctly different. Platelets that adhered to the Pd-glass surfaces were monolayered and well-spread without aggregation, whereas those adherent on Ti64 were partially aggregated, less spread and featured long filopodia (extended membrane protrusions; see Section 2.3 for a more detailed evaluation of platelet morphology). An increasing number of platelets adhered to the Pd-glass surfaces for time points up to 32 min of incubation, eventually covering the majority of the surface area. The onset of fibrin formation, however, was only observed for the 48 min time point. Notably, it

appears that the formation of fibrin fibers was only initiated after the adhesion of a second layer of platelets on top of the monolayered platelets and after occasional platelet aggregation.

In contrast, the Ti64 surfaces were covered by a dense fibrin network already after 16 min of incubation. Longer incubation times resulted in increasingly pronounced blood coagulation and thrombus formation, visible from the considerable fluorescence intensity (FI) of FG, marking the fibrin network (Figure 1E), and increasing presence of platelet aggregates (Figure 1D). Corresponding investigations via SEM support the observations made by CLSM for both materials (Figure S2A, Supporting Information).

The significantly reduced blood coagulation on the Pd-glass surfaces compared to the Ti64 surfaces was confirmed quantitatively by significantly ($p < 0.001$) lower concentration values of FG for all time points (Figure 1E). The activation state of adhered platelets was assessed by quantification of CD62P, which is a prominent marker for platelet activation expressed on the platelet membrane. While CD62P expression stayed at a low and roughly constant level for the Pd glass within the investigated incubation time range (Figure 1F), it reached a significantly ($p < 0.01$) higher level on Ti64 compared to the Pd glass already after 16 min and steadily increased further. Last, no differences for the activation of the complement system were observed, evaluated from the levels obtained for the complement compound C5a (Figure S2C, Supporting Information). Overall, benchmarking of the Pd glass clearly demonstrated its superior blood compatibility compared to Ti64.

2.2. Role of the Material's Atomic Structure: Blood Response to Amorphous and Crystalline Pd Samples

The material structure has been reported to influence the material–matter interaction at different time and size scales, ranging from environmental-species adsorption of oxygen or water,[34] over protein adsorption and conformation,[35] to cell adhesion.[36] Links between material structure and blood response have been reported primarily for polymers[37] and semiconductors,[38] for which structural differences impose differences in the material's electronic properties. In fact, the superior blood compatibility of semiconducting amorphous hydrogenated silicon carbide (a-SiC:H) coatings has been explained by a change in electron-transfer efficiency from fibrinogen to the material surface, suppressing contact activation.[39] For metals, in contrast, a rapid electron transfer is guaranteed irrespective of the material's atomic order, making differences in blood response as a function of material structure unlikely.

Nevertheless, when reaching out to other application fields such as catalysis, we find evidence that the structural characteristics of Pd-based metallic alloys impact the adsorption of oxygen and water,[34] which present the initial material–matter interaction events, and in turn may influence downstream protein and cell interactions.

With Pd glass being amorphous and Ti64 being crystalline in nature, we therefore scrutinized the potential impact of the materials' atomic structure on the thrombogenic properties. To this end, a crystalline counterpart to the amorphous Pd glass was produced via annealing. To assure full crystallinity, the annealing temperature was first determined by differential scanning calorimetry (DSC). **Figure 2**A shows the resulting thermal response of the as-cast Pd glass, which reveals a distinct exothermic peak at about 425 °C, ascribed to a crystallization process with the onset of crystallization (T_x) at about 420 °C.

Accordingly, and with the aim of obtaining high crystallinity, samples were heated to 460 °C, which corresponds to the end of the main crystallization peak. The sample's crystallinity was confirmed by XRD, the resulting pattern of which shows distinct Bragg peaks (Figure 2B, bottom). Microstructural investigations showed the presence of precipitated phases, obvious from the different grey tones in the BSE contrast (inset to Figure 2A), which is indicative of different chemical compositions. The phases are finely dispersed and distributed homogeneously. While further heating resulted in phase coarsening and thus a considerably stronger lateral chemical inhomogeneity (not shown), the fine microstructure of the sample heated to 460 °C was considered sufficiently homogeneous to serve as crystalline reference material.

As-cast and annealed samples were incubated in partially heparinized whole human blood and evaluated for platelet adhesion (actin), platelet activation (CD62), and fibrin formation (assessed via labeled fibrinogen, resulting in stained fibrin). Figure 2C shows representative CLSM images obtained after 8, 16, and 48 min of incubation, and quantified fluorescence intensities of the immunohistochemical markers (D) actin and (E) fibrinogen are shown in Figure 2D,E.

The blood response toward both sample types followed the same trend as the Pd samples in their amorphous state (Figure 1) and is described in detail above. Briefly, on both surfaces the number of adhered platelets increased over time (Figure 2C,D), with a fibrin network being only observed at the longest incubation time (48 min, Figure 2C). Quantification showed a slight increase of both markers, actin and fibrin, after 16 min and distinct increase of fibrin after 48 min (Figure 2E). Extent and time required for fibrin network formation, as well as the level of actin and FG, were comparable between as-cast and annealed samples. Complementary SEM analysis showed a comparable platelet morphology upon their adhesion to either surface (see insets to Figure 2C, and complementary SEM analysis for all time points in Figure S3, Supporting Information).

Overall, while a detailed analysis of the role of metal atomic structure in specific blood-component behavior is beyond the scope of this study, we ruled out a potential impact of Pd's underlying microstructure on the overall thrombogenicity. Consequently, the origin of reduced thrombogenicity of the Pd glass is likely to have a chemical origin.

2.3. Role of Chemistry: Blood Response to Different Metallic Glasses

To elucidate the impact of chemical surface composition on blood coagulation, a selection of chemically different BMGs was investigated. More specifically, a Ti-based and a Zr-based metallic glass were chosen in addition to the Pd-based one and compared with crystalline Ti64. Additionally, DLC coatings,

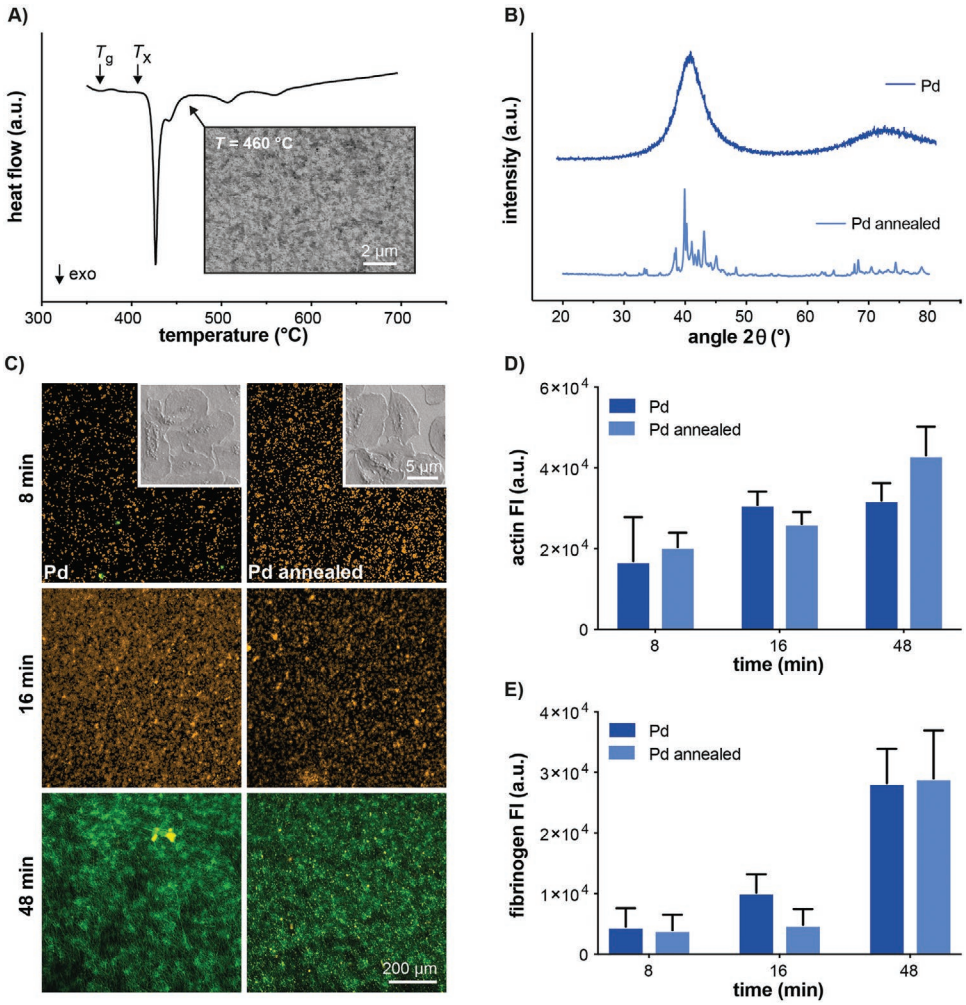

Figure 2. Role of the material's atomic structure in blood response. A) Thermal response of Pd glass upon heating, analyzed by DSC; inset to (A): SEM-BSE image of the annealed metal microstructure resulting from heating to 460 °C at a rate of 20 K min^{-1}. B) XRD patterns, showing the amorphous and crystalline structure of the as-cast and annealed Pd glass, respectively. C) CLSM images of immunofluorescence staining of platelet cytoskeletal actin (orange) and fibrin (green) for increasing incubation time in whole blood for $n = 3$ individual experiments and donors. Insets to (C): SEM-SE images of adhered platelets, showing their characteristic morphology at 8 min incubation time. D,E) Quantified fluorescence intensities (FI) per sample area for D) actin and E) fibrinogen, following increasing immersion times in whole human blood for $n = 2$ individual experiments and donors.

which are likewise amorphous and present the current gold standard in blood-contacting surfaces with low thrombogenicity,[2,40] were included as reference material.

As to the BMGs, we chose $Ti_{40}Zr_{10}Cu_{32}Pd_{14}Sn_4$[41] and $Zr_{52.5}Cu_{17.9}Ni_{14.6}Al_{10}Ti_5$,[42] because both base elements, Ti and Zr, and their alloys are well-accepted biometals, with a reportedly high corrosion resistance in physiological liquids exceeding that of Ti64.[43,44] Moreover, these compositions are known to have a fairly high glass-forming ability, concomitant with a high critical casting thickness D_c of 10[41] and 16 mm,[42] respectively, and can thus be prepared in bulk form. As to the mechanical properties, the reader is referred to Table S1, Supporting Information, where we provide, in comparison to crystalline Ti64, an overview of the mechanical properties characteristic for the bulk metallic glasses investigated in this study.

Prior to blood incubation, the material microstructure and physicochemical surface state were characterized, and the amorphous nature of all metallic glasses was verified by XRD (**Figure 3**A, left). The surface chemical composition was analyzed via X-ray photoelectron spectroscopy (XPS), and their relative compositions are summarized in Figure 3A, center. The carbon signal is attributed to contamination. As expected from the materials' nominal bulk compositions and the elements' intrinsic oxidative nature, the surfaces of Ti64 and of the Ti and Zr glasses are characterized by a considerable oxygen content related to various possible oxides forming readily with Ti and Zr, and also with Al (for Ti64 and the Zr glass) or Cu (for the Ti and Zr glasses). The surface oxygen content on the Pd glass is considerably lower (at only ≈5.5 at%), possibly related to oxides formed with Si and Cu, each of which has a surface concentration of roughly 2 at%, or unspecific oxygen adsorption (chemisorption) to the noble Pd, which presents the foremost element composing the material surface (≈89 at%).

The surface wettability was determined via water contact-angle measurements (WCA, Figure 3A, right) and was highest for Ti64,

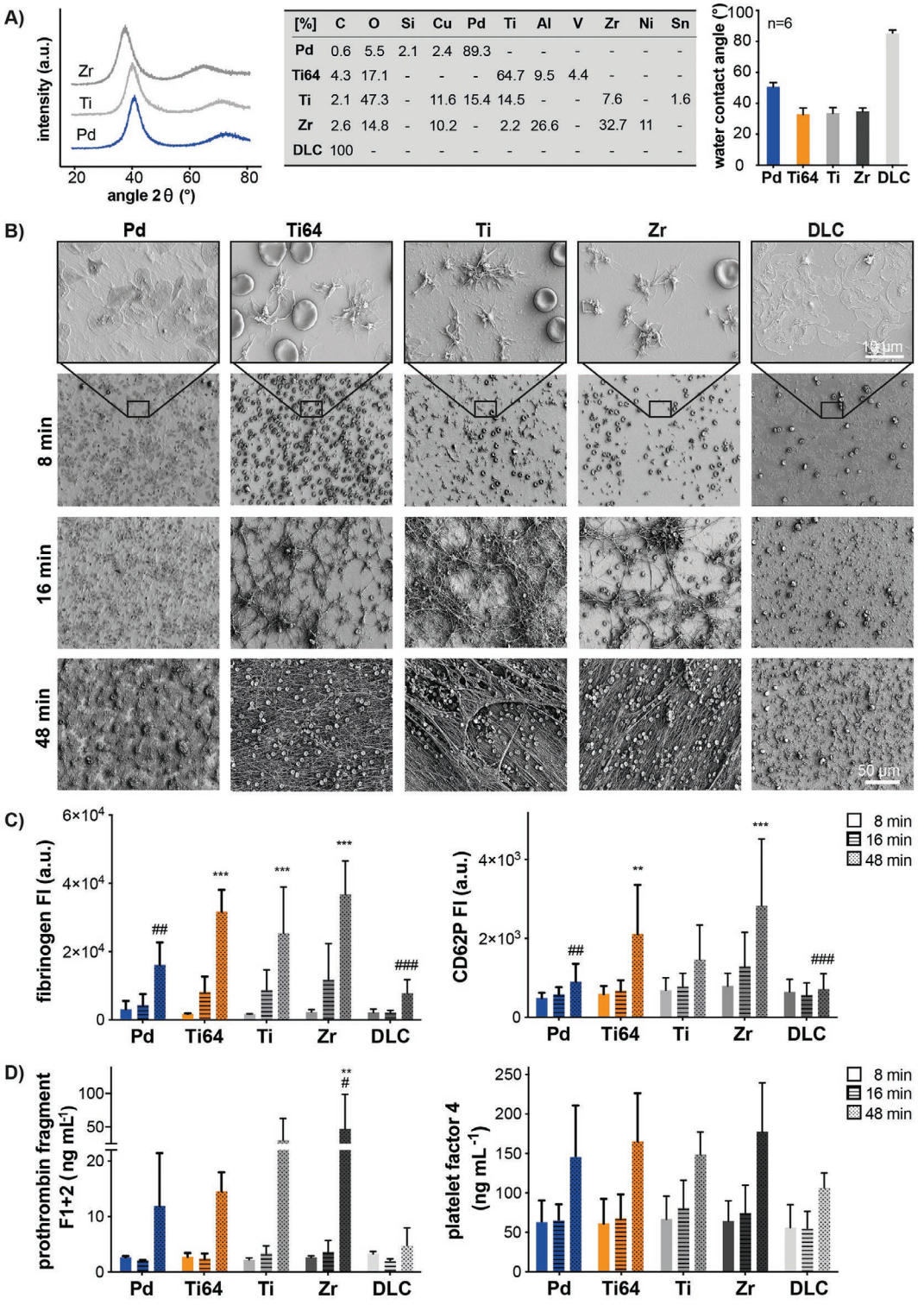

Figure 3. Impact of material chemistry on blood coagulation. A) Physicochemical material characterization; left: amorphous structure of the metallic glasses ($Pd_{77.5}Si_{16.5}Cu_6$, $Zr_{52.5}Cu_{17.9}Ni_{14.6}Al_{10}Ti_5$, and $Ti_{40}Zr_{10}Cu_{32}Pd_{14}Sn_4$ (in at%) as the Pd-, Zr-, and Ti-based metallic glasses, respectively), verified by XRD; center: surface chemistry characterized by XPS (in at%); right: surface wettability determined by static water contact-angle measurements. B) Temporally resolved SEM-SE images of platelet adhesion and fibrin network formation upon incubation in whole blood; top row: magnified views of adhered platelets showing their characteristic morphology after 8 min of incubation. C) Quantified fluorescence intensity (FI) per sample area determined by microarray scanning of fibrinogen and CD62P (platelet activation). D) Quantified biomolecular concentration in the supernatant determined by ELISA of F1+2 (coagulation activation) and PF4 (platelet activation). Data are presented as mean ± SD for $n = 4$. Asterisks and hash symbols present statistical significance compared to DLC: $^{**}p < 0.01$, $^{***}p < 0.001$ and Ti64: $\#p < 0.1$, $\#\#p < 0.01$, $\#\#\#p < 0.001$.

revealing the lowest contact angle at 32.9° ± 4.1°, corresponding to a hydrophilic surface, closely followed by those obtained for the Ti glass and Zr glass at 33.7° ± 3.6° and 34.9° ± 2.2°, respectively. While the WCAs of these three materials were at a comparable level, the one obtained for the Pd glass was notably higher at 50.8° ± 2.6°. The largest WCA, however, was obtained for DLC surfaces at 85.0° ± 2.4°, therewith presenting the least hydrophilic material among the ones investigated. Linking the WCA to the underlying surface chemistry suggests that increased wettability relates to exposed surface metal oxides, that is, to those associated with Ti64, and the Ti and Zr glasses. Notably, the surface roughness was comparable across all materials (Table S2, Supporting Information), which were prepared to a mirror-like surface finish. Based on this and our observation via SEM that blood responses did not differ at occasional scratches resulting from the mechanical surface finish, the influence of roughness as the origin of material-derived blood response differences was excluded.

Upon blood incubation, notable differences were observed between the materials tested: while after 8 min of incubation, platelet adhesion had occurred on the surfaces of all materials (Figure 3B, first and second row), the platelets' shape was distinctively different. Motivated by the long-lasting credo in material–blood interaction research that the morphology of adhered platelets relates to their activation status,[45] their morphology was analyzed in detail by SEM imaging (Figure 3B, first row).

Two groups can be distinguished according to the platelet morphology: In the first group, platelets on the Pd glass and DLC coatings were round and fully or almost fully spread, and only sporadically formed filopodia or aggregates. In the second group, platelets on Ti64 and the Ti and Zr glasses showed a low degree of spreading but formed multiple, long filopodia. Here, the filopodia extended to connect with each other, indicating early platelet aggregation.

The classification in these two groups stands firm for increasing incubation times (Figure 3B): on the group-1 materials (Pd, DLC), an increasing number of platelets adhered first in a monolayer until almost full surface coverage at 16 min of incubation, with no detectable sign of fibrin formation, followed eventually by adhesion of a second cell layer. Platelets adhering to pre-adhered ones showed low extent of spreading and extending filopodia, with only occasional signs of aggregation. No fibrin network formed on either the Pd glass or DLC after 16 min and only sporadically on the Pd glass after 48 min. In contrast, for the group-2 surfaces (Ti64, Ti, Zr), the platelets formed aggregates, and fibrin formation was initiated after 16 min of incubation, without reaching full material-surface coverage by the adhered platelets. On these materials, the fibrin network developed into a dense thrombus after 48 min. The observations made by SEM imaging with respect to both platelet morphology/coverage and fibrin-network formation are supported by analogue observations via immunohistochemical analysis (see Figure S4, Supporting Information).

Additionally to the qualitative analysis by SEM and CLSM, the blood response to the different material surfaces was assessed quantitatively via immunohistochemical staining and microarray scanning of FG and CD62P (Figure 3C), and via ELISA for the soluble markers prothrombin fragment F1+2 and platelet factor PF4 (Figure 3D). While F1+2 is a prominent marker for the generation of active thrombin, PF4 is released from activated platelets.[46] The amount of FG and all coagulation–activation markers steadily increased with incubation time for all materials, as expected from any artificial material in contact with blood. The respective absolute levels of all markers were lowest for the DLC surfaces, followed by those for the Pd glass. Upon 48 min of incubation, the highest mean levels for all markers were detected for the Zr glass, followed by the Ti-based materials, that is, Ti64 and Ti glass. Accordingly, the concentration of platelet-activation markers of both, those adhered to the surface (CD62, Figure 3C) and present in the supernatant (PF4, Figure 3D), was lowest for the DLC substrates, followed by the Pd glass. Again, the highest levels, that is, the strongest platelet activation, were detected for the Zr glass. However, no significant difference in the concentration of the TAT complex or complement-activation marker C5a between the materials was found (see Figure S4C,D, Supporting Information).

Research into hemocompatibility of inorganic materials indeed already showed the poor performance of Ti and Zr. Ti induced macroscopic clot formation and stronger platelet binding and activation compared to PVC and stainless steel,[47] whereas Zr was described as an intermediate activator compared to Ti.[48] While this seems to contradict our findings of highest thrombogenicity for the Zr-based glass, prediction of the biological responses for multi-component alloys is much more challenging. In this regard, a thin-film Zr glass ($Zr_{53}Cu_{33}Al_9Ta_5$) was shown to reduce platelet attachment and aggregation compared to a sputter-coated, that is, presumably amorphous, Ti surface.[49] Similar to our findings, the platelets on both materials, that is, the Zr-glass and Ti coating, showed low spreading and aggregation. Similarly, low platelet spreading was observed upon adsorption from platelet-rich plasma (PRP) to a Ni-free Zr-based glass ($Zr_{48}Cu_{45}Al_7$) with varying additions of silver, and to pure Zr used as a reference.[25] The authors concluded from a low count of adhered platelets and a low hemolytic rate that the materials were hemocompatible. A number of further studies came to the same conclusion on the hemocompatibility of the investigated glasses based on Zr ($Zr_{56}Al_{16}Co_{28}$)[22] or Ti ($Ti_{60}Nb_{15}Zr_{10}Si_{15}$),[50] though in neither study thrombogenicity or any biomolecular markers were addressed, nor were the materials benchmarked against gold-standard materials used in clinics.

Our data puts these findings into a new perspective. By comparing the Zr- or Ti-based materials to DLC and Pd glass, we show that the differences between the Zr- and Ti-based metals are insignificant in their difference when compared to DLC and Pd glass. In fact, all materials tested based on Zr or Ti were considerably thrombogenic and as such appear unsuitable for their use in direct contact with blood.

Our results are in line with those reported by Huang et al.,[51] who compared crystalline Ti and DLC surfaces and found greater platelet adhesion and aggregation on Ti surfaces compared to DLC. However, in contrast to our findings, they observed platelet spreading to be greater on Ti and concluded that greater spreading indicates higher platelet activation on Ti, though without assessing platelet activation on a molecular level. This link between platelet morphology and its activation

state appears to be a dogma in literature, as a higher degree of spreading is generally considered to correspond to a higher level of platelet activation.[45,52–54] Based on this, many studies have been considering platelet spreading as a direct marker for surface-induced blood activation and waived any biomolecular evidence.[40,55] Our results, however, show that platelet activation does not necessarily correlate with platelet morphology. In fact, we observed the highest level of platelet activation, assessed through CD62P (Figure 3C), for the Zr glass and Ti64 on which platelet spreading was low (Figure 3B), whereas we identified the lowest level of activation for the Pd glass and DLC on which platelets spread the most.

In an attempt of explaining blood or blood-component responses toward biomaterials, the surface wettability is often considered.[40,49,56–58] The materials' hydrophilicity is then related to platelet adhesion and spreading, and ultimately to the materials' hemocompatibility—thus far with no coherence across different studies. For instance, the superior performance of DLC was explained by its lower hydrophilicity compared to Ti,[40] while a higher hydrophilicity was stated to improve hemocompatibility for surface-treated Si:DLC coatings.[56] Additionally, reduced platelet adhesion was related to low hydrophilicity of Zr-based amorphous thin films compared to pure Ti coatings,[49] but to high hydrophilicity of functionalized Ti surfaces.[57] Finally, while some studies related high hydrophilicity to greater platelet spreading, and interpreted it as a high activation state,[40,58] our results show the opposite with the least hydrophilic materials inducing the highest levels of platelet adhesion and spreading, but lowest levels of platelet activation. Interestingly, reports on hydrophobic polymeric surfaces demonstrated high platelet adhesion and spreading in the early stages of blood response, which as a dense monolayer covered the biomaterial surface and inhibited further thrombogenic events.[59,60] This "passivation phenomenon" appears to be in line with our observations on Pd glass and DLC surfaces, and their relative lower hydrophilicity compared to the group-2 materials. However, the monolayer of platelets adhered to polymeric surfaces was activated, strongly opposing our observation of low activation on both, Pd-glass and DLC surfaces. For the inorganic materials investigated in this study, we report a consistent trend for the materials' wettability (Figure 3A) and their thrombogenicity, both following Ti64/Ti/Zr < Pd < DLC (Figure 3). It further appears that the surface-oxygen content (Figure 3A) follows the same trend, indicating a possible link between these surface parameters. However, despite the unquestioned relevance of wettability on blood responses, and the distinct differences in surface parameters between the materials, these results do not yet allow concluding on possible mechanisms behind the superior performance of Pd over the state-of-the-art metal Ti64.

2.4. Initiation of Coagulation Cascade: Fibrinogen Adsorption, Conformation, and Subsequent Platelet Adhesion

For a mechanistic understanding of the largely superior blood response observed for Pd glass compared to Ti64, we performed a detailed analysis of the platelet-adhesion profile and the underlying material–protein interactions. The latter present the early events in material–biological matter interactions and initiation of the coagulation cascade. More specifically, motivated by the observed differences in hydrophilicity levels between group 1 and 2 materials and the well-known relation between hydrophilicity and protein orientation,[61] we dissected in detail the conformation of fibrinogen upon its adsorption to the surfaces, and related it to the platelets' adhesion pattern and their activation.

FG is the third most abundant blood serum protein. While soluble in blood in its inactive state, FG adsorbs rapidly to biomaterial surfaces upon their contact with blood. Adsorption of FG on biomaterial surfaces is a critical early event of blood interaction with implanted devices, and thus pivotal for their thrombogenicity. Once adsorbed, FG can facilitate the adhesion of platelets and by that trigger their (partial) activation, which in turn triggers the release of coagulation factors, further upregulating the platelet activation and ultimately initiating thrombus formation.[62] Because of its key role in triggering the coagulation cascade, particular attention must be devoted to the initial stage of FG interaction with the biomaterial surface, with regard to both the amount and conformation with which FG adsorbs on the respective surface.[52,58]

Structurally, FG has two sets of three nonidentical polypeptide chains: Aα, Bβ, and γ.[63] Especially important for the FG–platelet interaction are the two γ-chain carboxyl termini, which present the main receptor-recognition motif for the platelet integrin $\alpha_{IIb}\beta_3$ (also known as glycoproteins GPIIb/IIIa), and present the main mediator for platelet binding.[58,64] Binding to $\alpha_{IIb}\beta_3$ mediates platelet adhesion and aggregation, and further initiates a series of intracellular signaling events, leading to changes in platelet morphology, with more bonds to γ-chains resulting in greater platelet spreading.[65] In this light, it has been recognized that the accessibility of the $\alpha_{IIb}\beta_3$ recognition sites on the γ-domains directly depends on the conformation of the FG molecules adhering to the surface.[52,66,67]

Here, two FG conformations are distinguished upon FG's anchoring on a surface and schematically presented in **Figure 4**A: in "conformation 1" (Figure 4A, top), FG adheres to the substrate with its α-domains, thus rendering its γ-chains accessible for the binding through the platelets' $\alpha_{IIb}\beta_3$ integrins. In "conformation 2" (Figure 4A, bottom, left and right), FG adheres with its γ-chains facing the material surface, therewith hindering their accessibility for the binding of platelets via integrin $\alpha_{IIb}\beta_3$. While no exclusive conformation can be expected for a given surface (as illustrated in Figure 4A, bottom), we aimed at analyzing the predominant conformation type characteristic for Pd glass and Ti64.

Quantification of the total adsorbed FG concentrations (Figure 4B) revealed considerably lower levels on top of the Pd-glass compared to the Ti64 surfaces upon their immersion in FG buffer solution for 30 min. Yet, notably, the concentration of accessible FG γ-chains was ≈1.4-fold higher on Pd-glass compared to Ti64 surfaces, as established using a custom-made ELISA (Figure 4B). Particularly considering the overall lower FG amount on Pd glass, the data clearly show that Pd-glass surfaces favor FG "conformation 1" (Figure 4A, top) more strongly than Ti64 surfaces. Consequently, a higher degree of platelet adhesion and activation is expected on the Pd glass.

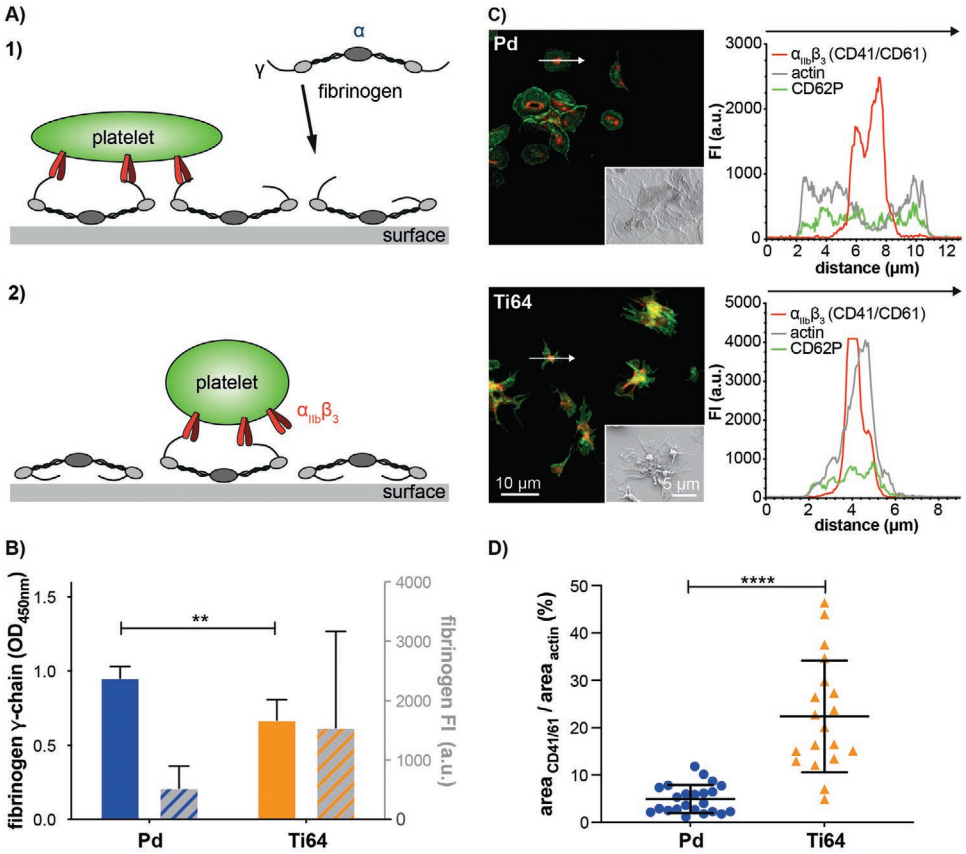

Figure 4. Fibrinogen adsorption, γ-chain accessibility, and platelet adhesion on Pd glass and Ti64. A) Schematic presentation of platelet–FG interaction as a function of the possible FG conformations upon adsorption on biomaterial surfaces. Platelet binding and spreading occurs mainly through their $\alpha_{IIb}\beta_3$ integrin interacting with the γ-chains of adhered FG. Higher accessibility of γ-chains relates to higher platelet binding and spreading. B) Quantification of total adsorbed FG via determination of the FI of fluorophore-labeled FG (light grey, right axis), and quantification of accessible FG γ-chains on the samples' surfaces determined via a custom-made ELISA (left axis); data are presented as mean ± SD for $n = 3$–4. Asterisks denote statistical significance as follows: $^{**}p < 0.01$. C) CLSM images of adherent platelets on Pd glass and Ti64 after 8 min of incubation in PRP and subsequent staining for $\alpha_{IIb}\beta_3$ (visualized using CD41/CD61 integrin) (red), actin (grey), and CD62P (green). Insets: magnified SEM-SE images of adherent platelets. Right: representative line profiles for the FI of CD41/CD61, actin and CD62P across adhered platelets (corresponding lines are marked in the CLSM images with white arrows). D) Quantified area occupied by CD41/CD61, normalized to the area occupied by actin. The area ratio gives a measure of the CD41/CD61 distribution across the platelets (mean ± SD). Asterisks denote statistical significance as follows: $^{****}p < 0.0001$.

To address this hypothesis, the resulting platelet interaction with the surfaces and in particular the platelets' activation following their adhesion was assessed through the expression of CD62P and active $\alpha_{IIb}\beta_3$ on the platelet surfaces. The analysis was conducted on a single-cell level via immunohistochemical staining and CLSM. Both proteins are found on the surface of activated platelets while CD41/CD61 ($\alpha_{IIb}\beta_3$) is the major receptor for FG. Generally, inactive $\alpha_{IIb}\beta_3$ is present in resting, in non-activated platelets in the plasma membrane, and in α-granules. Upon platelet activation, the integrin undergoes an inside-out conformational change, which allows its binding to FG.[68,69] Importantly, the surface-anchored FG suffices to trigger outside–in activation of $\alpha_{IIb}\beta_3$ integrin, that is, a conformational change of $\alpha_{IIb}\beta_3$, which in turn facilitates platelet activation. Besides its role in binding to FG, $\alpha_{IIb}\beta_3$ also plays a role in platelet-to-platelet interaction and platelet aggregation, and eventually in initiating thrombus formation.[68,70,71] The determination of $\alpha_{IIb}\beta_3$ integrin expressed on the platelet surface thus allows assessing the activation status of platelets. To this end, a CD41/CD61 antibody, which binds specifically to the activated conformation of $\alpha_{IIb}\beta_3$, was used. Figure 4C shows the cell morphology and surface distribution of CD62P and CD41/CD61 on adherent platelets. Actin was additionally stained to mark the platelets' surface area. The representative line profiles in Figure 4C show a close correlation of the CD62P signal and the actin signal for both materials, concomitant with a homogeneous expression profile across the entire cell surface. In contrast, CD41/CD61 expression was found to be notably different between the surfaces, with CD41/CD61 densely clustering in the center of the fully spread platelets on the Pd glass, but homogeneously distributed over the entire (smaller) cell area on Ti64 (Figure 4C). Quantification of the area covered by CD41/CD61 and normalized to the area occupied by actin (as a measure for the surface of spread platelets) confirmed a significantly ($p < 0.0001$) lower CD41/CD61 coverage of the platelet surfaces on those adhered to the Pd glass compared to those adhered to Ti64 (Figure 4D).

Considering the role of $\alpha_{IIb}\beta_3$ integrins in platelet-to-platelet interactions, we assume that the chance for interaction is

higher on Ti64, on which the adhered cells have more CD41/CD61 per surface area (Figure 4D) and have a volumetric, nonflat morphology, that is, larger free surface area. The apparently higher number of platelets on Ti64 (Figure S2, Supporting Information), concomitant with a higher total surface area occupied by adhered platelets in spite of lower spreading, may further stimulate platelet interaction. On the contrary, while the cells on Pd glass promote adhesion of a second platelet layer (Figure 1), and thus provide evidence that some CD41/CD61 integrin is expressed at the free surface, their characteristic clustered integrin pattern only provides a locally restricted surface region for possible platelet interactions. This and the rather flat cell shape potentially make binding through integrin interactions with free platelets in the media less likely. These considerations may thus explain the higher degree of platelet aggregation observed on Ti64 (and other "group 2" materials, Figure 3B) compared to the Pd glass. We assume that amongst potential other pathways, the FG conformation, and the CD41/CD61 distribution in adhered platelets resulting from it, present a mechanism responsible for the observed platelet aggregation and thrombus formation on Ti64 but not on Pd-glass surfaces. Platelet aggregation on Ti64 may have been further stimulated through filopodia, which are known to regulate platelet–matrix and platelet–platelet adhesive interactions,[61] being visible for platelets adhered to Ti64, but not when adhered to Pd.

Platelet aggregation is linked to coagulation through initiation of platelet coagulant activity via the expression of negatively charged membrane phospholipids (phosphatidyl serine, PS), which catalyze clot formation.[72] Different platelet subpopulations have been described based on the expression/presentation of PS, $\alpha_{IIb}\beta_3$ and CD62P. While an anti-correlation between PS and $\alpha_{IIb}\beta_3$ has been described for platelets adhering on glass, also PS+/$\alpha_{IIb}\beta_3$+ populations have been reported.[72] Interestingly, expression/presentation of PS, $\alpha_{IIb}\beta_3$ and CD62P is highly dependent on the type of stimulation, on calcium levels and—most importantly for the current study—on the surface that platelets adhere to.[72,73] For example, platelets were shown to be positive for PS, CD62P and $\alpha_{IIb}\beta_3$ when adhering to glass, but triple-negative when adhering to TiO_2 surfaces in calcium-free buffer.[73] Notably, PS and CD62P but not $\alpha_{IIb}\beta_3$ expression could be induced on TiO_2 when increasing intracellular calcium levels.[73] In view of these reports we hypothesize that the Pd glass and DLC surfaces induce the formation of a distinctly different platelet sub-population when compared to Ti64 (and other "group 2" materials). However, as platelet populations are considered snapshots of transient stages that are capable of interconversion,[72,73] further research in this direction is needed and foreseen for the here described materials and for engineered materials in general.

Overall, the monolayered coverage of platelets on Pd and DLC may be described as a passivation layer, shielding the material form contact with blood components, as described before for polymers.[59,60] Using biomolecular methods to probe the activation state, we show that—different from polymeric surfaces—the platelets forming this passivation layer have a low activation status, and by probing the platelet–platelet interaction provide a rational for subsequent reduced platelet aggregation.

Our observations on the adsorption and orientation of adherent FG (Figure 3B) further show that not the FG quantity but its orientation (that influences γ-chain accessibility) impacts thrombogenicity, which is in good agreement with previous reports by others.[52,74–77] Literature in fact suggests that FG quantity and its conformation are tightly linked, as the amount of adsorbed FG can impact its conformation upon adsorption.[52,78] It has further been suggested that conformational changes of FG can already be induced by the surface adhesion process, which suffices to expose different platelet-binding domains.[66] Both, amount and conformation of adhered FG, have been understood to depend largely on the physicochemical surface state, including its wettability.

In terms of total FG adsorption, a lower hydrophilicity was reported to favor FG adsorption[52,61,78] along with increased platelet adhesion, but slower thrombus formation.[61] While our data support an apparent relation between low hydrophilicity and increased platelet adhesion and retarded thrombus formation, lower levels of total adhered FG were found on the Pd glass albeit its lower hydrophilicity compared to Ti64. This finding was consistent throughout all materials tested, with both group-1 material surfaces, that is, Pd glass and DLC, showing the least hydrophilic surfaces (Figure 3A) and lower amount of FG compared to Ti64 and the other group-2 material surfaces (Figure 3C). Our findings are supported by observations of Jones et al.,[40] who not only reported lower FG levels adsorbed on DLC coatings compared to Ti surfaces, but also explained the greater hemocompatibility of DLC with its lower hydrophilicity. Even though the Pd glass studied here is significantly more hydrophilic than DLC (Figure 3A), it exhibits the least hydrophilic surface of all glasses analyzed in this study. Its wettability may thus contribute to the superior performance of the Pd glass.

Surface wettability is also understood to play a role in surface-induced conformational changes through triggering unfolding of FG.[58,78] More specifically, FG is considered to adsorb with its hydrophilic and hydrophobic domains most strongly to alike surfaces.[58] It should be noted that unfolding does not necessarily promote platelet binding unless the conformational change renders the binding sites accessible. This direct relationship was demonstrated by Zhang et al.[58] for the adsorption to hydrophilic and hydrophobic polymer substrates. In their study, wettability dictated not only FG adsorption with their respective domains, either exposing the platelet binding sites or rendering them inaccessible, but also impacted the resulting platelet adhesion. Similarly, our results reveal a direct dependence of the FG conformation first on the accessibility of platelet-binding sites through $\alpha_{IIb}\beta_3$ integrin, and ultimately on the platelet adhesion patterns (Figure 3B,C). However, while in the above mentioned study on polymeric substrates, hydrophilicity promoted the adsorption via FG's α-region and thus the exposure of γ-chains for effective platelet binding,[58] our results on metallic surfaces suggest the opposite, namely promotion of a favorable configuration for platelet binding on Pd with lower hydrophilicity compared to Ti64 (Figures 3A and 4B). This contrasting result may origin from fundamental differences between the materials classes, that is, polymeric and metallic surfaces, particularly in light of their impact on protein interaction. It thus highlights the necessity for a comprehensive consideration of the physicochemical surface properties—extending beyond surface

wettability assessment—of the materials under investigation for blood-contacting devices.

Finally, we revisit the wide discussion on platelet spreading regarded as a hallmark of platelet activation and a widely accepted paradigm in the field of blood compatibility, as discussed in Section 2.3. Possible material–cell interactions leading to platelet spreading were also discussed, particularly in light of surface wettability. Here, we showed that despite greater spreading, platelet aggregation and other biochemical indicators of platelet activation, such as CD62P and PF4 concentrations, were lower on Pd than on Ti64. This breaks with the current dogma that spreading would equal activation, and is further supported by our results on CD41/CD61 as an additional marker for platelet activation, which confirm that their activation state is significantly reduced when adhered on Pd glass. The observed morphological differences of adhered platelets, namely a flat cellular shape versus a granular shape on Pd-glass and Ti64 surfaces, respectively (Figure 3B first row), may be rationalized through the differences in predominant FG conformation between the materials and the resulting density of accessible γ-chains. This proposes a possible link between the accessibility of γ-chains and the ability of platelet spreading, as also inferred from literature,[65] and schematically outlined in Figure 4A.

Being a limitation of our study, the reported blood response was analyzed in a closed system under semi-static conditions, in which released biomolecular activation markers accumulate over time. This may lead to signal amplification and consequently in an artificial acceleration in the speed of consecutive events in the blood-response pathways. In fact, in light of the absence of clearance, the amplitude of responses in an in vitro model is regarded a worst-case scenario in hemocompatibility assessment of biomaterials.[79] In terms of the hydrodynamic simplification, however, previous results on blood compatibility of polymeric substrates with varying surface chemistries assessed under flow were found to be in line with results under static conditions.[58] It can thus be expected that the here observed distinct differences in blood response are also maintained under dynamic conditions.

In summary, we propose that platelet adhesion and spreading are influenced by the inherent chemical nature of the Pd glass, concomitant with a low surface oxygen content and a relatively low hydrophilicity compared to Ti64. However, we do not directly assign platelet spreading to an activated state of platelets, as is generally reported in literature, because the biochemical indicators suggest otherwise.

3. Conclusion

In this study, we investigated a Pd-based metallic glass for its potential as a metallic bulk material for blood-contacting devices without coating. Brought in contact with partially heparinized whole human blood, it showed a remarkably high resistance to thrombus formation compared to medical-grade crystalline Ti64, the state-of-the-art metal used in circulatory support systems. Compared to Ti64, Pd-glass substrates stimulate increased platelet spreading, but reduced platelet aggregation and significantly reduced activation (assessed by platelet activation factors such as CD62P, PF4, and CD41/CD61). This hinders fibrin formation on the Pd surfaces and therewith leads to an overall lowered thrombogenicity. Comparison of the Pd glass with its crystalline counterpart did not reveal any significant differences in the blood response, suggesting that the observed effect is not due differences in crystallinity. Further comparison to other metallic glasses based on Zr and Ti suggests that it is the chemistry of the Pd glass, and presumably the linked higher hydrophobicity, that is responsible for its low thrombogenicity.

We attribute the superior properties of the Pd glass to processes following the conformational change of adsorbed FG, where Pd favors a higher accessibility of FG γ-chains for $\alpha_{IIb}\beta_3$ integrins, thus leading to enhanced platelet spreading but reduced platelet aggregation due to a decreased density of expressed $\alpha_{IIb}\beta_3$ integrin per cell area. This sheds new light on an old problem, where the amount of protein concentration was thought to govern hemocompatibility. Overall, our results show that the configuration of FG determines the effective amount of platelet adsorption and activation, which in turn decides on the fate of the material in contact with blood. This contradicts existing literature, where most reports deal with either FG conformation or amount in isolation. Future studies may focus on other proteins and biomolecular factors present in whole blood and their resulting potential effect on FG adsorption and platelet responses. This will be particularly important when considering kinetic aspects, for example the time available for adsorption during which various blood proteins compete.

Benchmarked to the gold-standard of low-thrombogenic coatings, namely DLC, our results show that DLC remains the material with the lowest thrombogenic potential. However, since Pd glass can be produced in bulk form (as thick as 15 mm), it overcomes the limitations associated with DLC coatings, such as the risk of crack formation and coating flake-off. Last, the superior mechanical performance of metallic glasses makes the Pd glass particularly interesting for devices under pulsatile elastic load. In fact, with respect to its high strength, low Young's modulus and high energy that can be stored elastically, the mechanical properties of the $Pd_{77.5}Si_{16.5}Cu_6$ glass outperform those of crystalline Ti64 (Table S1, Supporting Information), and even more so those of ceramics and polymers. This suggests an immense potential of bulk Pd glass for blood-contacting devices such as mechanical circulatory support systems.

4. Experimental Section

Reference alloy: Medical grade Ti–6Al–4V (in wt%, Ti64) (5 mm extruded rod, extra-low interstitial grade; ASTM F-136, ASTM B-348) was purchased from L. Klein SA (Biel, Switzerland) and used as reference material.

Metallic Glass Synthesis: The compositions of the metallic glasses investigated were as follows: Pd-based with composition $Pd_{77.5}Si_{16.5}Cu_6$ (in at%), Zr-based known as "Vit105"—one of the most investigated BMGs with composition $Zr_{52.5}Cu_{17.9}Ni_{14.6}Al_{10}Ti_5$ (in at%),[42] and Ti-based with composition $Ti_{40}Zr_{10}Cu_{32}Pd_{14}Sn_4$ (in at%).[41] All master alloys were prepared by melting high-purity metals in an arc melter (Edmund Bühler GmbH, Germany) in high-purity Ar atmosphere. The Pd master alloy was subsequently processed following the protocol described in ref. [32], which entails boron-oxide (B_2O_3) fluxing to reduce oxides and heterogeneous nucleation, and thus to increase the critical casting

thickness. The Pd and Zr glasses were suction-cast into 5 mm rods using water-cooled copper molds and then sawed into 1 mm thick discs. The Ti glass was tilt-cast into 3 mm thick plates and discs of 5 mm diameter with 1 mm thickness were prepared by electric spark-erosion cutting.

Annealing: To create a crystalline reference to the Pd glass, the latter was heated at 20 K min^{-1} to 460 °C and kept for 5 min. This temperature was chosen from preceding DSC sweeps (Mettler-Toledo DSC1/700) at 20 K min^{-1} heating rate, which revealed ≈420 °C as the crystallization onset temperature and 460 °C as the end temperature of the main crystallization peak.

Sample Preparation: All samples except the DLC-coated ones were prepared freshly 1 day prior to each blood-incubation experiment by mechanically grinding and polishing (water-based silica polishing suspension, Buehler, USA) to a mirror surface finish (roughness comparable across all materials, see Table S2, Supporting Information), followed by ultrasonic cleaning first in water and then in isopropanol.

DLC Coating: Thin a-C:H films, referred to as DLC, were deposited on polished Ti64 substrates using RF (13.56 MHz) plasma-activated chemical vapor deposition with acetylene (C_2H_2) as process gas. As an adhesion-promoting layer an ≈90 nm thick silicon-containing DLC layer was deposited in situ prior to the DLC deposition using tetramethylsilane (TMS, $Si(CH_3)_4$). The base pressure in the chamber was set at $\leq 10^{-5}$ Pa. Prior to deposition, the substrates were cleaned by ultrasonication in an ethanol/acetone mixture, and additionally in vacuum using an Ar plasma for 30 min operated at 2.5 Pa and −600 V sample self-bias. Thereafter, without interruption of the plasma, the Ar-gas flow was stopped while TMS was introduced at 0.5 Pa using again −600 V self-bias. Keeping the plasma discharge at −600 V, TMS was substituted by 1 Pa C_2H_2. The resulting film thickness was 320 nm.

X-Ray Diffraction: The alloys' microstructure was characterized by XRD analysis (PANalytical X'Pert diffractometer, PANalytical, the Netherlands) using monochromated Cu K_α radiation (45 mA, 40 kV) and a 2θ range of 20° to 80°.

Scanning Electron Microscopy: SEM imaging was carried out using a Hitachi SU-70 SEM. For investigation of the alloys' microstructure, imaging was performed at 5 kV acceleration voltage in BSE mode, which was sensitive to atomic-number (Z) contrast, thus revealing the chemical distribution.

Water Contact Angle: The surface wettability was assessed by measuring the WCA, using a drop-shape analysis system (DSA100, KRÜSS GmbH) and applying the sessile-drop technique. WCA measurements were carried out at RT using Milli-Q water, and the WCA values were obtained using the tangent-fitting method. The WCA results were averaged over six measurements made on six independent samples for each material.

X-Ray Photoelectron Spectroscopy: The surface chemistry was measured using XPS on a PHI 5000 VersaProbe II instrument (USA) equipped with a monochromatic Al K_α X-ray source. The energy resolution was set to 0.8 eV $step^{-1}$ at a pass energy of 187.85 eV for survey scans, and to 0.125 eV $step^{-1}$ and 29.35 eV pass energy for high-resolution region scans. Ar sputtering was performed for 60 s (2 kV, 2 υm), leading to an estimated depth of 10 nm. C 1s at 284.5 eV was used as a calibration reference to correct for charge effects. To correct for the O 1s/Pd $3p_{3/2}$ interference, Pd $3p_{1/2}$ was used to obtain the oxygen concentration. Data analysis was performed using the CasaXP software (Casa Software Ltd, UK).

Blood Incubation: Human whole blood from healthy volunteers (ethical approval BASEC No. PB_2016-00816 from the local ethics committee) was withdrawn into S-Monovette tubes (neutral S-Monovette, Sarstedt AG, Germany) by a standard venipuncture technique, partially heparinized (0.43 IU mL^{-1}) and used within 1 h after withdrawal. For analysis of platelet adhesion, PRP was isolated by centrifugation of the whole blood at 200g for 20 min. Sample incubations were performed identically for whole blood and PRP.

Immediately prior to the incubation in blood or PRP, the samples were immersed in 70% ethanol for 5 min and dried in a laminar-flow clean bench. The material samples were then placed into custom devices made of PTFE (Teflon), overlayed with 2.8 mL of whole blood or PRP, closed with a PTFE lid, sealed with Parafilm to avoid blood–air contact, and placed on an orbital shaker (Polymax, Heidolph) at 10 rpm. Separate devices were used for different sample types and incubation time points.

At distinct time points (8, 16, 24, 32, 48 min) the blood was removed from the samples and transferred to centrifuge tubes, followed by immediate stabilization with ethylenediaminetetraacetic acid (EDTA) (Sigma-Aldrich) at a final concentration of 5 mM. Blood plasma was isolated by centrifugation at 2000g for 10 min and stored at −80 °C until further analysis. The sample disks were carefully washed three times with PBS using an orbital shaker (10 rpm) for 1 min each, transferred into 96-well plates and fixed either for 30 min in 4% PFA/PBS solution (Sigma-Aldrich) for subsequent immunofluorescence staining or for 1 h in Karnovsky solution (4 g paraformaldehyde, 50 mL MilliQ water, 5 mL glutaraldehyde 50%, 45 mL PBS without glucose, pH 7.4) (all Sigma-Aldrich) for SEM analysis. The entire procedure was carried out at RT.

Sample Preparation for Scanning Electron Microscopy: Fixed samples were dehydrated using an ascending ethanol series, fixed in hexamethyldisilazane for 30 min, and finally sputter-coated with an ≈10 nm Au layer for electron conductivity (SCD 030, Bal-Tec AG, Liechtenstein). Cell morphology and blood coagulation were qualitatively investigated by SEM imaging (Hitachi SU-70), performed at 5 kV acceleration voltage in secondary-electron (SE) mode.

Immunofluorescence Staining and Imaging: For CLSM, fixed samples were blocked via incubation in 5% goat serum and 1% FCS in PBS for 1 h. Activated platelets were stained with CD62P-selectin Alexa Fluor 647 antibody (1:100, BioLegend). Cells were permeabilized for 10 min in 0.1% Triton X 100 and actin-stained with phalloidin–Alexa Fluor 546 conjugate (1:200, BioLegend) for 1 h. To follow FG adhesion and subsequent fibrin formation, FG–Alexa Fluor 488 conjugate (final concentration of 18 µg mL^{-1}) was supplemented to the blood prior to sample incubation, thereby allowing for the visualization of fibrin fibers that incorporate labeled FG.

To investigate platelet adhesion to the different substrates and platelet activation upon incubation of the samples in PRP, fixed samples were incubated in FcR-blocking solution (BioLegend) for 10 min. The adherent platelets were stained with CD62P-selectin Alexa Fluor 488 antibody (1:100, BioLegend) and CD41/CD61 Alexa Fluor 647 antibody (PAC-1, 1:100, BioLegend) for 1 h. Cells were then permeabilized for 10 min in PBS-containing 0.1% Triton X 100 and washed. The actin cytoskeleton was stained with Alexa Fluor 546 (1:200, BioLegend) for 1 h. All antibodies were dissolved in 1% FCS/PBS. All staining procedures were performed at RT, and all antibody incubation steps were followed by threefold washing with PBS. Images were taken with a LSM780 confocal microscope (Carl Zeiss AG, Switzerland). Fluorescence intensities (FIs) were quantified with a fluorescence microarray scanner (LS ReloadedTM, Tecan Trading AG, Switzerland).

To assess the coverage of CD41/CD61 on the platelets, the area occupied by CD41/CD61 integrin and actin was used and their ratio determined. ImageJ software (v 1.53c, Wayne Rasband, NIH, USA) was deployed to create a macro that splits the fluorescence channels, sets the signal threshold (Otsu's thresholding method), and finally calculates the thresholded area.

Molecular Markers of the Coagulation Cascade: Selected molecular markers of the coagulation cascade were analyzed in EDTA-stabilized plasma using commercially available ELISAs. Platelet activation (platelet factor 4 (PF4), Thermofisher), coagulation activation (Prothrombin Fragment 1+2 (F1+2), USBio; TAT complex, Abcam), and complement activation (C5a, Abcam) were assessed according to the manufacturers' instructions.

Surface Interaction with Plasma Proteins: To quantify FG adsorption and assess the γ-chain accessibility of adsorbed FG, the Pd and Ti64 surfaces were incubated in PTFE well plates with FG–Alexa Fluor 647 conjugate (100 µg mL^{-1}; Thermofisher) dissolved in PBS for 30 min. After washing, FG γ-chain antibody (1:200, IgG2a, [4H9], GeneTex) was added and samples were incubated for 2 h. Following washing, goat anti-mouse IgG2a secondary antibody biotin (1:300, Thermofisher) was added and incubated for 1 h. Following washing, Streptavidin-HRP (1:500, Abcam) was added. After 30 min incubation, the samples were washed, transferred into a 96-well plate and washed again. 3,3′,5,5′-tetramethylbenzidine substrate (Abcam) was added to each well

and the reaction stopped after 10 min using stop solution (Abcam). The solution was then transferred into a new 96-well plate and its absorbance measured at 450 nm (Mithras2 Plate reader, Berthold Technologies). All antibodies were dissolved in ELISA buffer (Dil N, Abcam). All washing steps were repeated four times using ELISA wash buffer (Abcam), and all incubations were performed on an orbital shaker. The entire procedure was performed at RT.

For FI quantification of FG adsorption, samples were analyzed with a fluorescence microarray scanner, performed as described above. FI values were determined from the obtained images via ImageJ software, evaluating the samples' inner 80% surface area.

Statistical Analysis: All data were analyzed using GraphPad Prism (GraphPad Software Inc., USA) either by Students *t*-test (two-tailed) (comparison of Pd with Ti64) or by a one-way ANOVA and Tukey post-hoc test. Asterisks denote statistical significance as follows: $*p < 0.05$, $**p < 0.01$, $***p < 0.001$, $****p < 0.0001$. All data were presented as mean values ± standard deviation (SD).

Supporting Information

Supporting Information is available from the Wiley Online Library or from the author.

Acknowledgements

M.C. and E.M. contributed equally to this work. The authors thank Fabian Haag and Christian Wegmann from LMPT/ETH for their support in metallic glass casting and instrumental assistance, Nicole Kleger from Complex Materials/ETH for acquisition of the roughness data, and Yvonne Elbs-Glatz, Stefanie Guimond, and Ursina Tobler from the Biointerface lab/Empa for their support in the blood experiments. This study was conducted as part of the Zurich Heart project of Hochschulmedizin Zurich. Financial support by the Uniscientia foundation, Vaduz, Switzerland is gratefully acknowledged. Y.C. received support from the EMPAPOSTDOCS-II program, which is funded by the European Union's Horizon 2020 research and innovation program under the Marie Skłodowska-Curie grant agreement 754364.

Open access funding provided by Eidgenossische Technische Hochschule Zurich.

Conflict of Interest

The authors declare no conflict of interest.

Data Availability Statement

The data that supports the findings of this study are available in the supplementary material of this article.

Keywords

blood-contacting devices, coagulation, hemocompatibility, metallic glass, palladium, platelet activation, thrombogenicity

Received: August 18, 2021
Revised: September 21, 2021
Published online: October 17, 2021

[1] B. D. Ratner, *Biomaterials* **2007**, *28*, 5144.
[2] D. Ufukerbulut, I. Lazoglu, in *Biomaterials for Artificial Organs*, (Eds: M. Lysaght, T. J. Webster) Elsevier, **2011**, pp. 207–235.
[3] M. Walkowiak-Przybyło, L. Klimek, W. Okrój, W. Jakubowski, M. Chwiłka, A. Czajka, B. Walkowiak, *J. Biomed. Mater. Res., Part A* **2012**, *100*, 768.
[4] D.-C. Sin, H.-L. Kei, X. Miao, in *Coatings for Biomedical Applications*, (Ed: M. Driver), Elsevier, New York **2012**, pp. 264–283.
[5] E. A. Rose, H. R. Levin, M. C. Oz, O. H. Frazier, Q. Macmanus, N. A. Burton, E. A. Lefrak, *Circulation* **1994**, *90*, II87.
[6] A. Koster, M. Loebe, R. Sodian, E. V. Potapov, R. Hansen, J. Müller, F. Mertzlufft, G. J. Crystal, H. Kuppe, R. Hetzer, *J. Thorac. Cardiovasc. Surg.* **2001**, *121*, 331.
[7] K. Yamazaki, P. Litwak, O. Tagusari, T. Mori, K. Kono, M. Kameneva, M. Watach, L. Gordon, M. Miyagishima, J. Tomioka, *Artif. Organs* **1998**, *22*, 466.
[8] R. Hauert, K. Thorwarth, G. Thorwarth, *Surf. Coat. Technol.* **2013**, *233*, 119.
[9] D. Coleman, J. Lawson, W. J. Kolff, *Artif. Organs* **1978**, *2*, 166.
[10] J. F. Löffler, *Intermetallics* **2003**, *11*, 529.
[11] J. F. Löffler, *Z. Metallkd.* **2006**, *97*, 225.
[12] W. L. Johnson, *MRS Bull.* **1999**, *24*, 42.
[13] W. Peter, R. Buchanan, C. Liu, P. Liaw, M. Morrison, J. Horton, C. Carmichael Jr, J. Wright, *Intermetallics* **2002**, *10*, 1157.
[14] F. Qin, X. Wang, S. Zhu, A. Kawashima, K. Asami, A. Inoue, *Mater. Trans.* **2007**, *48*, 515.
[15] A. Greer, K. Rutherford, I. Hutchings, *Int. Mater. Rev.* **2002**, *47*, 87.
[16] H. F. Li, Y. F. Zheng, *Acta Biomater.* **2016**, *36*, 1.
[17] B. Zberg, P. J. Uggowitzer, J. F. Löffler, *Nat. Mater.* **2009**, *8*, 887.
[18] P. Tsai, Y. Lin, J. Li, S. Jian, J. Jang, C. Li, J. Chu, J. Huang, *Intermetallics* **2012**, *31*, 127.
[19] G. Praveen Kumar, M. Jafary-Zadeh, R. Tavakoli, F. Cui, *J. Biomed. Mater. Res., Part B* **2016**, *105*, 1874.
[20] M. Jafary-Zadeh, G. Praveen Kumar, P. S. Branicio, M. Seifi, J. J. Lewandowski, F. Cui, *J. Funct. Biomater.* **2018**, *9*, 19.
[21] L. Huang, C. Pu, R. K. Fisher, D. J. Mountain, Y. Gao, P. K. Liaw, W. Zhang, W. He, *Acta Biomater.* **2015**, *25*, 356.
[22] R. Wang, Y. Wang, J. Yang, J. Sun, L. Xiong, *J. Non-Cryst. Solids* **2015**, *411*, 45.
[23] H.-H. Huang, Y.-S. Sun, C.-P. Wu, C.-F. Liu, P. K. Liaw, W. Kai, *Intermetallics* **2012**, *30*, 139.
[24] W. Diyatmika, C.-C. Yu, Y. Tanatsugu, M. Yasuzawa, J. P. Chu, *Thin Solid Films* **2019**, *688*, 137382.
[25] H. Li, Y. Zheng, F. Xu, J. Jiang, *Mater. Lett.* **2012**, *75*, 74.
[26] J. C. Wataha, K. Shor, *Expert Rev. Med. Devices* **2010**, *7*, 489.
[27] B. Woodward, *Platinum Met. Rev.* **2012**, *56*, 213.
[28] M. Hulander, J. Hong, M. Andersson, F. Gervén, M. Ohrlander, P. Tengvall, H. Elwing, *ACS Appl. Mater. Interfaces* **2009**, *1*, 1053.
[29] H. Chen, D. Turnbull, *Acta Metall.* **1969**, *17*, 1021.
[30] C. Pampillo, *Scr. Metall.* **1972**, *6*, 915.
[31] K.-F. Yao, Y.-Q. Yang, N. Chen, *Intermetallics* **2007**, *15*, 639.
[32] D. Granata, E. Fischer, V. Wessels, J. F. Löffler, *Acta Mater.* **2014**, *71*, 145.
[33] International Organization for Standardization (ISO), *10993 Biological Evaluation of Medical Devices—Part 4: Selection of Tests for Interactions with Blood*, International Organization for Standardization, Geneva **2002**.
[34] V. Hasannaeimi, S. Mukherjee, *Sci. Rep.* **2019**, *9*, 12136.
[35] L. A. Buchanan, A. El-Ghannam, *J. Biomed. Mater. Res., Part A* **2010**, *93*, 537.
[36] J. Schroers, G. Kumar, T. M. Hodges, S. Chan, T. R. Kyriakides, *JOM* **2009**, *61*, 21.
[37] N. Kawamoto, H. Mori, M. Terano, N. Yui, *J. Biomater. Sci., Polym. Ed.* **1997**, *8*, 859.
[38] M. F. Maitz, M.-T. Pham, E. Wieser, I. Tsyganov, *J. Biomater. Appl.* **2003**, *17*, 303.
[39] A. Bolz, M. Schaldach, *Artif. Organs* **1990**, *14*, 260.
[40] M. Jones, I. McColl, D. Grant, K. Parker, T. Parker, *J. Biomed. Mater. Res.* **2000**, *52*, 413.

[41] S. Zhu, X. Wang, A. Inoue, *Intermetallics* **2008**, *16*, 1031.
[42] X. Lin, W. Johnson, W. Rhim, *Mater. Trans. JIM* **1997**, *38*, 473.
[43] X. B. Huang, N. M. Lin, R. Q. Hang, B. Tang, J. W. Qiao, *Mater. Sci. Forum* **2013**, *745–746*, 754.
[44] F. Qin, X. Wang, G. Xie, S. Zhu, A. Kawashima, K. Asami, A. Inoue, *Mater. Trans.* **2007**, *48*, 167.
[45] J. E. Aslan, A. Itakura, J. M. Gertz, O. J. McCarty, in *Platelets and Megakaryocytes*, (Eds: J. M. Gibbins, M. P. Mahaut-Smith), Springer, New York, NY **2012**, pp. 91–100.
[46] C. Sperling, M. Maitz, C. Werner, in *Hemocompatibility of Biomaterials for Clinical Applications*, (Ed: C. A. Siedlecki), Elsevier, New York **2018**, pp. 77–104.
[47] J. Hong, J. Andersson, K. N. Ekdahl, G. Elgue, N. Axen, R. Larsson, B. Nilsson, *Thromb. Haemostasis* **1999**, *82*, 58.
[48] J. Hong, A. Azens, K. N. Ekdahl, C. G. Granqvist, B. Nilsson, *Biomaterials* **2005**, *26*, 1397.
[49] C.-H. Chang, C.-L. Li, C.-C. Yu, Y.-L. Chen, S. Chyntara, J. P. Chu, M.-J. Chen, S.-H. Chang, *Surf. Coat. Technol.* **2018**, *344*, 312.
[50] S. T. Rajan, A. Bendavid, B. Subramanian, *Colloids Surf., B* **2019**, *173*, 109.
[51] Y. Huang, X. Lü, M. Jingwu, N. Huang, *Appl. Surf. Sci.* **2008**, *255*, 257.
[52] B. Sivaraman, R. A. Latour, *Biomaterials* **2010**, *31*, 832.
[53] S. Goodman, M. Lelah, L. Lambrecht, S. L. Cooper, R. Albrecht, *Scan. Electron Microsc.* **1984**, *1984*, 279.
[54] S. N. Rodrigues, I. C. Gonçalves, M. Martins, M. A. Barbosa, B. D. Ratner, *Biomaterials* **2006**, *27*, 5357.
[55] Y. Ding, Z. Yang, C. W. Bi, M. Yang, S. L. Xu, X. Lu, N. Huang, P. Huang, Y. Leng, *ACS Appl. Mater. Interfaces* **2014**, *6*, 12062.
[56] R. K. Roy, H. W. Choi, J. W. Yi, M.-W. Moon, K.-R. Lee, D. K. Han, J. H. Shin, A. Kamijo, T. Hasebe, *Acta Biomater.* **2009**, *5*, 249.
[57] M. A. Alfarsi, S. M. Hamlet, S. Ivanovski, *Dent. Mater. J.* **2014**, *33*, 749.
[58] L. Zhang, B. Casey, D. K. Galanakis, C. Marmorat, S. Skoog, K. Vorvolakos, M. Simon, M. H. Rafailovich, *Acta Biomater.* **2017**, *54*, 164.
[59] L. M. Szott, C. A. Irvin, M. Trollsas, S. Hossainy, B. D. Ratner, *Biointerphases* **2016**, *11*, 029806.
[60] C. L. Haycox, B. D. Ratner, *J. Biomed. Mater. Res.* **1993**, *27*, 1181.
[61] C. Sperling, M. Fischer, M. F. Maitz, C. Werner, *Biomaterials* **2009**, *30*, 4447.
[62] B. Furie, B. C. Furie, *N. Engl. J. Med.* **2008**, *359*, 938.
[63] M. Mosesson, *J. Thromb. Haemostasis* **2005**, *3*, 1894.
[64] N. P. Podolnikova, V. P. Yakubenko, G. L. Volkov, E. F. Plow, T. P. Ugarova, *J. Biol. Chem.* **2003**, *278*, 32251.
[65] M. Jiroušková, J. K. Jaiswal, B. S. Coller, *Blood* **2007**, *109*, 5260.
[66] B. Sivaraman, R. A. Latour, *Biomaterials* **2011**, *32*, 5365.
[67] A. Chiumiento, S. Lamponi, R. Barbucci, *Biomacromolecules* **2007**, *8*, 523.
[68] S. J. Shattil, H. Kashiwagi, N. Pampori, *Blood* **1998**, *91*, 2645.
[69] D. Varga-Szabo, I. Pleines, B. Nieswandt, *Arterioscler., Thromb., Vasc. Biol.* **2008**, *28*, 403.
[70] S. P. Jackson, *Blood* **2007**, *109*, 5087.
[71] Y. Zhang, Y. Qiu, A. T. Blanchard, Y. Chang, J. M. Brockman, V. P.-Y. Ma, W. A. Lam, K. Salaita, *Proc. Natl. Acad. Sci. USA* **2018**, *115*, 325.
[72] A. Donati, S. Gupta, I. Reviakine, *Biointerphases* **2016**, *11*, 029811.
[73] S. Gupta, A. Donati, I. Reviakine, *Biointerphases* **2016**, *11*, 029807.
[74] M. Rottmar, E. Müller, S. Guimond-Lischer, M. Stephan, S. Berner, K. Maniura-Weber, *Dent. Mater.* **2019**, *35*, 74.
[75] D. M. Hylton, S. W. Shalaby, R. A. Latour Jr, *J. Biomed. Mater. Res., Part A* **2005**, *73*, 349.
[76] I. Firkowska-Boden, C. Helbing, T. J. Dauben, M. Pieper, K. D. Jandt, *Langmuir* **2020**, *36*, 11573.
[77] J. L. Brash, T. A. Horbett, R. A. Latour, P. Tengvall, *Acta Biomater.* **2019**, *94*, 11.
[78] P. Roach, D. Farrar, C. C. Perry, *J. Am. Chem. Soc.* **2005**, *127*, 8168.
[79] W. Van Oeveren, *Scientifica* **2013**, *2013*, 392584.